C. R. Chimie 17 (2014) 839–848

Contents lists available at ScienceDirect

Comptes Rendus Chimie

www.sciencedirect.com

Full paper/Mémoire

In situ synthesis and characterization of TiO_2/HPM cellulose hybrid material for the photocatalytic degradation of 4-NP under visible light☆

Mohamed Faouzi Nsib [a,*,b], Faten Hajji [a], Asma Mayoufi [a], Noomen Moussa [a,b], Ali Rayes [a,b], Ammar Houas [a]

[a] URCMEP (UR11ES85), Faculty of Sciences, University of Gabès, 6029 Gabès, Tunisia
[b] National School of Engineers (ENIG), University of Gabès, 6029 Gabès, Tunisia

ARTICLE INFO

Article history:
Received 10 November 2013
Accepted after revision 14 January 2014
Available online 29 March 2014

Keywords:
TiO_2
Cellulose
Hybrids
Photodegradation
Visible light

ABSTRACT

Hybrid TiO_2–hydroxypropyl methyl cellulose (TiO_2–HPMC) nanophotocatalysts were prepared by a simple in situ synthesis. The weight ratios of HPMC-to-TiO_2 were 5, 10 and 20%, respectively. The as-prepared nanocomposites were characterized by XRD, XPS, UV–vis DRS, ATG and BET surface area analysis. Surface morphology was assessed by the means of SEM. The photocatalytic degradation of 4-nitrophenol (4-NP) in neutral aqueous solution under visible light irradiation was examined to evaluate the efficiency of the hybrids in comparison to pure TiO_2. The results indicated that the in situ hybridization of TiO_2 with HPMC significantly increases its specific surface area and extends its light absorption range to the visible region. Consequently, TiO_2–HPMC nanocomposites were photocatalytically much more active than pure TiO_2. Moreover, the TiO_2–HPMC hybrids were found to be sufficiently photostable after five experimental runs.

1. Introduction

The removal of commercial stains from industrial wastewaters is a great concern topic for environment safety. During the last years, advanced oxidation processes (AOPs) such as UV/H_2O_2, ozonation, (photo)Fenton, sonolysis, electrochemical oxidation, and photocatalysis have been widely and extensively explored to mitigate a great variety of pollutants present in various environmental media. AOPs have been considered as alternatives to conventional water treatment technologies. Among many AOPs, photocatalysis using light and inorganic materials (oxides) has received huge attention as one of the most viable environmental cleanup technologies.

Today, nanomaterials and hybrid materials based on organic and inorganic components represent a wide range of innovative tools in materials science [1–8]. Generally, inorganic components display interesting mechanical, thermal, magnetic, electrical (and so on) properties, whereas organic components are associated with ease of implementation, elastic, optical, electrochemical and biological properties... Thanks to the nearly infinite choice of their formulations, the potential of hybrid materials is immense [9,10].

Specifically, hybrid materials derived from the combination, at the nanoscale size, of a polymer with an inorganic phase constitute a large part of the nanocomposite materials based on a polymer [11]. This kind of material has a great interest, for two main reasons. On the one hand, the combination of these two phases with opposite properties can lead to a variety of materials with new properties intermediate between those of polymers and inorganic materials [12]. On the other hand, the

☆ Thematic issue dedicated to François Garin.
* Corresponding author.
E-mail address: mohamed.faouzi.ncib@gmail.com (M.F. Nsib).

1631-0748/$ – see front matter
http://dx.doi.org/10.1016/j.crci.2014.01.010

diversity of production processes and synthesis routes opens the perspective to generate an "infinity" of multifunctional materials [13–17]. As a result, hybrid materials open up new possibilities in various application domains such as catalysis, coatings, membranes, optics, purification and storage of gas, drug delivery, and information storage [18–21].

Particularly in photocatalysis, TiO_2 is an excellent photocatalyst [22,23]. However, it has two major flaws that can be partially solved by modifying its structure. First, this semiconductor absorbs light at wavelengths below 390 nm, making it weakly active under solar irradiation. However, it is possible to act on this feature by modifying the TiO_2 network. The second weakness of titanium dioxide is its low specific surface area. For example, the reference material, the P25 marketed by Degussa, has a surface area of about 50 $m^2 g^{-1}$. To be fully effective, photocatalysis requires a large surface area, synonymous with high surface contact between the photocatalyst and the oxidized species.

Thus, various strategies have been adopted to improve the photocatalytic efficiency of TiO_2. They can be summarized as morphological changes, such as increasing the specific surface area and porosity, and chemical changes by incorporating additional components in the structure of TiO_2. Although the photocatalytic activity of TiO_2 under visible or solar light requires chemical modifications, the overall performance should be greatly enhanced by improving its morphology.

The association of TiO_2 with a functional polymer in a hybrid material is expected to improve its morphology [24]. In addition, organic molecules allow better coverage of the solar emission spectrum, especially when the organic and inorganic networks are interpenetrating. Thus, the hybrid entity should benefit from the synergistic effects of physical and chemical interactions that occur between organic and inorganic components and may therefore be used as a photocatalyst for efficient degradation of toxic pollutants under visible and solar lights.

Cellulose is the most abundant natural polymer in the world. It can be regenerated or derived to produce many useful products, because it is renewable, biodegradable, and biocompatible [25–27]. Moreover, cellulose and its derivatives are relatively low-cost products. Thus, taking into account the mild conditions of the sol–gel process, the ease of synthesis can promote continuous preparation of hybrid nanocomposites for various industrial applications, in particular for photocatalysis.

Although, in the last years, considerable work has been reported on the preparation of mineral-polymer nanocomposites [28,29], the literature dealing with the preparation of hybrid nanocomposites as photocatalysts based on cellulose derivatives is quite scarce [30–32].

The aim of this research is the preparation and characterization of novel organic–inorganic hybrid nanomaterials with high photocatalytic properties. These nanomaterials are based on titanium dioxide and polyhydroxylated polymers such as cellulose derivatives. We made this choice because the polyhydroxylated polymers adsorb easily on the surface of the metal oxide layer and then provide free hydroxyl groups on which are adsorbed the metal alkoxides [33]. Thus, it is possible to extend the area of the sol–gel process and to alternate the adsorption of the polyhydroxylated organic compounds and of the metal alkoxides. This structure is expected to increase the surface area of the hybrids and to expand their wavelength response to reach the visible range. As a result, TiO_2–HPMC hybrid materials are expected to have high photocatalytic activity compared with pure TiO_2 and may consequently be used as efficient catalysts in green wastewater purification.

On the other hand, nitrophenols are the most common organic pollutants in industrial and agricultural effluents. Particularly, 4-nitrophenol (4-NP) has been widely used in the production of pesticides, herbicides, dyes, drugs, and other industrial chemicals. Thus, this compound is often detected as a water pollutant as a result of its release in industrial effluents. Remediation of wastewaters containing such a pollutant is very difficult, since nitrophenol compounds are usually resistant to biological degradation. Recently, several studies [34–36] have been published about TiO_2-based hybrid nanomaterials, especially for in situ surface modification, which have been used for the photodegradation of 4-NP and organic pollutants. For this reason, 4-NP ($C_6H_5NO_3$, $M = 139.11$) was chosen to be the probe compound to qualify the photocatalytic efficiency of TiO_2–HPMC hybrid materials. The cellulose derivative used in this work was hydroxypropyl methylcellulose (HPMC) $(C_6H_{10}O_5)_n$ of molar mass equal to 8.17×10^4 (Scheme 1).

2. Experimental

2.1. In situ synthesis of TiO_2–HPMC hybrids

The TiO_2–HPMC photocatalysts were prepared by a new method through a modified sol–gel process. In a typical synthesis, 22.5 mL of anhydrous titanium isopropoxide $Ti(^iO–Pr)_4$ were added dropwise into a solution containing 60 mL of isopropanol under vigorous stirring. The solution was stirred for 10 min at 60 °C, before 3 mL of acetic acid as a catalyst were added. Stirring continued under the same conditions of temperature for 3 h to form a solution denoted A. A mixture of 8 mL of distilled water, 40 mL of isopropanol and a volume of an aqueous solution of HPMC was prepared as solution B. The used volume of HPMC solution corresponds respectively to 5, 10 and 20% of HPMC-to-TiO_2 weight ratios. The hydrolysis process was initiated by adding dropwise solution B to solution A under agitation. The resulting mixture was stirred for 3 h, a time period long enough for gelation to be achieved, and then aged for 24 h at 25 °C to be matured. The resultant gel was filtered and washed with isopropanol and water and then dried in an oven overnight at 40 °C and was finally left to complete drying at ambient temperature for 2 weeks. Thus, TiO_2–HPMC hybrid powders were finally obtained.

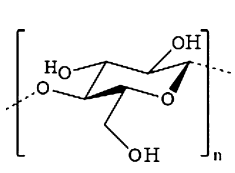

Scheme 1. Molecular structure of HPMC.

Pure TiO_2 was prepared using the same process, but without adding any aqueous solution of HPMC.

2.2. Catalyst characterization

The X-ray diffraction (XRD) patterns obtained with a Siemens HT/BT X-ray diffractometer using Cu Kα radiation at a scan rate of $0.02^\circ\ s^{-1}$ were used to decide the crystallite size and identity of TiO_2 powders. The average crystallite size was determined according to Scherrer's equation: $d = k\cdot\lambda/\beta\cdot\cos\theta$, where k is the shape factor of particles, equal to 0.89, β is the peak width at half-maximum (in radians), λ is the X-ray wavelength (0.15418 nm), and θ is the Bragg angle.

The scanning electron micrograph (SEM) was recorded with a Neoscope JCM-5000 (JEOL Company, Japan) electron microscope and was used for observing the shape and morphology of the prepared particles.

ESCALAB-210 spectrometer (VG Scientific) was used for X-ray photoelectron spectroscopy (XPS) measurements, the Al Kα X-ray source was operated at 300 W (15 kV, 20 mA). The surface properties of the TiO_2–HPMC sample were analyzed by recording the C 1s XPS spectra.

A UV–vis 3101 PC (UV Probe Shimadzu) was used to record the diffuse spectra (DRS) of the samples. Reflectance spectra were analyzed under ambient conditions in the 190–800-nm wavelength range.

The specific surface area of the catalysts was measured by N_2 adsorption using the BET isotherm with a Quantachrome autosorb-1.

TGA experiments of prepared pure TiO_2 and TiO_2–HPMC composites were performed with a SETERAM thermobalance, in the 20–500 °C temperature range, under a dynamic atmosphere of argon. The samples were put into platinum crucibles, at a heating rate of $10\ ^\circ C\ min^{-1}$.

2.3. Photodegradation experiments

Photocatalytic experiments were performed in an open Pyrex glass cell using 100 mL of an aqueous solution of 4-NP (10 ppm) as the model pollutant and 100 mg of as-prepared photocatalysts. The suspension was magnetically stirred in the dark for at least 30 min to ensure the establishment of the adsorption/desorption equilibrium. Then the light was turned on; this instant was treated as the starting point ($t = 0$) of the reaction. A 250-W halogen lamp with wavelength emissions (main range at 400–800 nm) was used as the visible light source. The lamp was positioned inside the photoreactor and its vessel was surrounded by a circulating water jacket to cool the reaction solution. At a defined time interval, samples of 1 mL were withdrawn from the suspension every sampling time during the irradiation. The photocatalysts were separated from the solution by centrifugation and the quantitative determination of 4-NP was performed by measuring its absorption at 401 nm (at pH 9) with a UV–vis spectrophotometer. A calibration curve was used to deduce the concentration of 4-NP. Total organic carbon (TOC) was determined by using a TOC-Ve Analyzer (Shimadzu) to follow the mineralization of 4-NP.

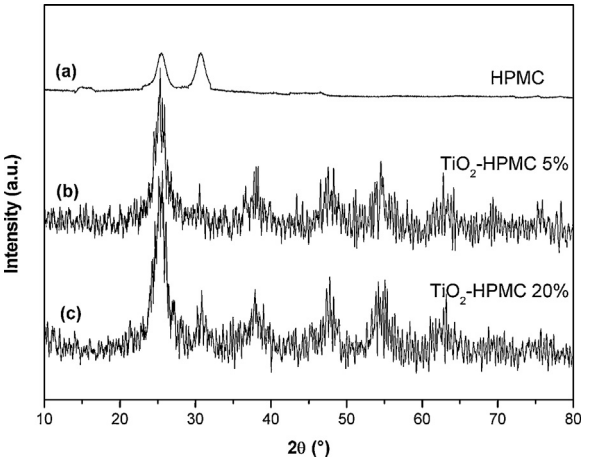

Fig. 1. Powder X-ray diffraction pattern of (a) HPMC, (b) TiO_2–HPMC 5%, and (c) TiO_2–HPMC 20%.

3. Results and discussions

3.1. XRD analysis of TiO_2–HPMC composite particles

As it is evident from Fig. 1, the wide-angle XRD patterns for the nanocomposite samples are dominated by the characteristic peaks of the anatase phase of TiO_2 and the HPMC. TiO_2 diffraction peaks at $2\theta = 25.7^\circ$, 37.9°, 47.8°, 55.1° and 64.2° match exactly (101), (004), (200), (105) and (204) reflections of the pure anatase phase, as reported in the literature [37], and no additional reflections belonging to other phases, such as rutile or brookite, are observed. These observations indicate that there is virtually no phase change in the TiO_2 structure after the process of in situ hybridization with HPMC. The crystalline structure of HPMC is characterized by both main peaks at positions $2\theta = 25.5^\circ$ and 30.7°. The first one is not found in the XRD pattern of the hybrid samples because it is overlapped with that of TiO_2 anatase peak at 25.7°, whereas the second one is clearly found. The relatively high width of the reflections associated with the TiO_2 phase suggests that the size of the particles is quite small. The average grain sizes are calculated using Scherrer's equation based on the full width at half-maximum of the (101) peak of the compounds. It is observed that the in situ hybridization of TiO_2 with HPMC reduced the grain size and enlarged the surface areas of nanoparticles. In fact, the particle sizes of pure TiO_2, TiO_2–HPMC 5%, and TiO_2–HPMC 20% are found to be 7.3 nm, 4.9 nm, and 5.3 nm, respectively. The smaller crystallite size indicates that the preparation method of the TiO_2–HPMC nanocomposite used in the present work under mild conditions may effectively prompt the crystallization and inhibit grain growth.

3.2. SEM characterization

In order to understand the surface morphology of the TiO_2–HPMC nanocomposite, surface SEM images were taken for HPMC, TiO_2, and TiO_2–HPMC nanocomposite (Fig. 2). Fig. 2a shows the HPMC cellulose SEM surface

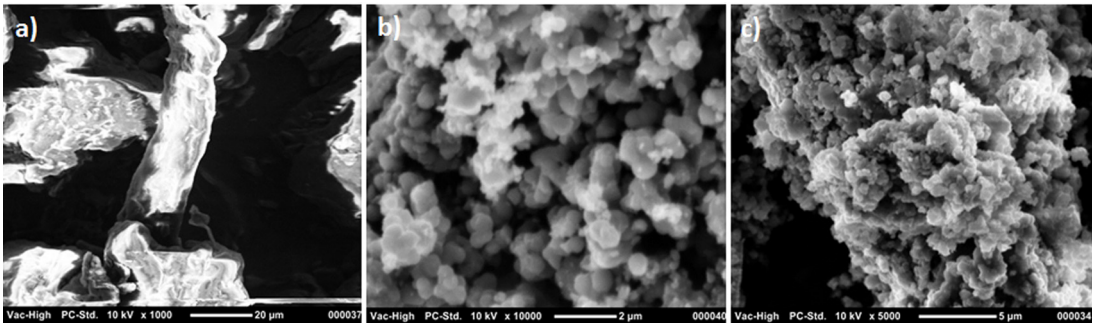

Fig. 2. SEM micrographs of (a) HPMC, (b) pure TiO_2, and (c) TiO_2–HPMC 5%.

image, which represents a smooth surface. The high-magnification SEM image shown in Fig. 2b reveals that pure TiO_2 particles are spherical, smooth, and separated from each other, but some aggregates of few particles are also shown. Fig. 2c shows a SEM image of the TiO_2–HPMC nanocomposite's surface, where it is observed that the surface is rough and has a spongy form; it looks as if small nucleuses had grown unevenly around TiO_2 particles. The particles do not have a well-defined morphology and the size is completely random. It is possible to observe that, in this case, small particles aggregate in large agglomerates. Fig. 2c also shows that the TiO_2 particles are densely distributed not only on the surface, but also in the cellulose matrix.

Based on SEM images, it is possible to conclude that the in situ hybridization of TiO_2 with HPMC has an influence on the surface morphology and nanocrystallites arrangements in the final aggregates.

3.3. BET characterization

In general, the surface area of the catalyst is the most important factor influencing catalytic activity. For an application to photodegradation, the materials are to be porous to permit adsorption of the pollutant to be degraded and not only help surface reactivity. The surface area of nanoparticles was determined using the nitrogen gas adsorption method. The nitrogen adsorption–desorption technique provides information on the porosity of the prepared materials: specific surface area (S_{BET}), pore volume (P_v) and mean pore size (Ø). Fig. 3 exhibits the N_2 isotherms of TiO_2–HPMC composites, which provide information about the structural properties and pore geometries of the materials prepared at various compositions of HPMC.

From Fig. 3, we find out that the adsorption isotherms are characterized by a gradual increase in the adsorbed amount when the relative pressure values (P/P_0) are below 0.6. For relatively higher pressures, the isotherms are characterized by saturation levels that are characteristic of mesoporous adsorbents in which there is a capillary condensation. The desorption process is not reversible in this case and is characterized by a hysteresis of desorption with respect to adsorption. Thus, the adsorption curves follow types IV and V according to the IUPAC classification related to mesopore size (20–500 Å). The hystereses are of type H2, characterizing intercommunicating mesopores. Moreover, adsorption and desorption branches did not close and such irreversibility is observed at the lowest equilibrium pressures. It was proved that unusual adsorption/desorption patterns arise from an inherent structural flexibility of such adsorbents [38]. This behaviour may also be explained as a result of the combination of thermodynamic and network effects arising from non-coincidental capillary evaporation and condensation within interconnecting pores of various sizes [39].

The textural properties of surface area, pore volume, and average mesopore diameter obtained from N_2 adsorption–desorption analysis are summarized in Table 1. It is obvious from the table that all the prepared hybrid samples have a very high surface area compared with that of pure TiO_2. It is the proof that the hybridization of TiO_2 with HPMC could increase significantly its surface area, but this increase is more important for the synthesized hybrid of the low-weight fraction of the organic part. And then, the surface area of TiO_2–HPMC 5% catalyst increases notably until 222 $m^2\,g^{-1}$. The HPMC could inhibit particle growth during drying because of mixed bond Ti–O–C, which could inhibit the interaction among Ti particles.

Beside the influence of the surface area of the catalyst, BET characterization shows that the hybridization of TiO_2

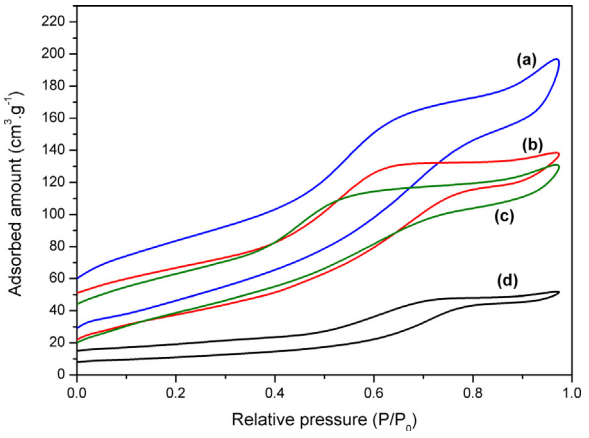

Fig. 3. (Color online). Nitrogen isotherms of TiO_2–HPMC *x*% hybrids, (a) $x = 5$, (b) $x = 10$, (c) $x = 20$, and (d) $x = 0$.

Table 1
N_2 adsorption–desorption data obtained from pure TiO_2 and TiO_2–HPMC hybrids. S_{BET}, S_{micro}, S_{meso}, P_v, $Ø_{meso}$ are BET surface area, surface of micropores, surface of mesopores, pore volume and mean mesoporous diameter, respectively.

Material	S_{BET} ($m^2\,g^{-1}$)	S_{micro} ($m^2\,g^{-1}$)	S_{micro} (%)	S_{meso} ($m^2\,g^{-1}$)	S_{meso} (%)	P_v ($cm^3\,g^{-1}$)	$Ø_{meso}$ (Å)
Pure TiO_2	53	40	75.5	13	24.5	0.08	215
TiO_2–HPMC 5%	222	145	65.3	77	34.7	0.32	143.3
TiO_2–HPMC 10%	179	111	62	68	38	0.22	108.4
TiO_2–HPMC 20%	188	102	54.3	86	45.7	0.21	83.2

with HPMC increases significantly the pore volume of catalyst. Particularly, it reaches 0.32 $cm^3\,g^{-1}$ for TiO_2–HPMC 5%, which is four times larger than that of pure TiO_2. Moreover, the proportion of mesoporous surface (S_{meso}) is found to increase with respect to the fraction of HPMC in the hybrid material. As a result, the mean size of the mesopores decreases from 215 Å for pure TiO_2 to attain 83.2 Å for TiO_2–HPMC 20%.

3.4. XPS analysis

This technique can be used to identify the nature of the transition metal species [40,41], which is important to understand the photocatalytic activity. Fig. 4 shows the typical high resolution of the C1s XPS spectra of as-synthesized TiO_2–HPMC 5% nanocomposite. The broader C1s peak region at 282–290 eV could be fitted to three line shapes with binding energies at 284.5, 286, and 288 eV. These different binding-energy peaks can be assigned to C–O, C=O, and O–C=O, respectively [42,43]. The binding energy at 284.5 eV may be assigned to disordered carbon in the hybrids [44], whereas the binding energies at 286 and 288 eV indicate the formation of carbonated species and a substitution of lattice titanium ions to form Ti–O–C bonding [39]. Under in situ hydrolysis and condensation reactions of the sol–gel process in the presence of HPMC molecular chains, Ti–O–C bonds can be formed through a dehydration reaction between the Ti–OH groups and the C–OH groups in HPMC molecular chains. Besides, it is well known that there are always some active OH groups located on the surface of nano TiO_2. Under drying conditions, these OH groups on TiO_2 surfaces can form Ti–O–C bonds with the C–OH groups in HPMC molecular chains. These Ti–O–C bonds are covalent bonds. Thus, the analysis of the C1s XPS spectra confirmed the formation of TiO_2–HPMC as an organic–inorganic hybrid nanocomposite.

3.5. UV–vis diffuse reflectance spectra (DRS)

UV–vis diffuse reflectance spectroscopy, which is generally used to detect the presence of framework- and non-framework-incorporated transition metal species in structures and to distinguish the coordination states of the metal ions [45,46], was used in this case to provide some insight into the interactions of the photocatalyst materials with photon energies.

Fig. 5 illustrated the UV–vis diffuse reflectance full spectra of bare TiO_2 and TiO_2–HPMC composite photocatalysts with different HPMC content. It is obvious that the bare TiO_2 absorbs light with wavelengths below 380 nm only. The spectrum of TiO_2 consists of a single absorption usually ascribed to charge transfer from the valence band (mainly formed by 2p orbitals of the oxide anions) to the conduction band (mainly formed by the $3d_{t2g}$ orbitals of the Ti^{4+} cations) [47]. After being sensitized by HPMC, the TiO_2–HPMC composite photocatalysts not only can strongly absorb the UV light, but also can absorb visible light. We observed a noticeable shift of the optical absorption edge for the TiO_2–HPMC systems towards the visible regions. Surely, this shift towards the longer wavelengths originates from the band gap narrowing of titanium dioxide by HPMC

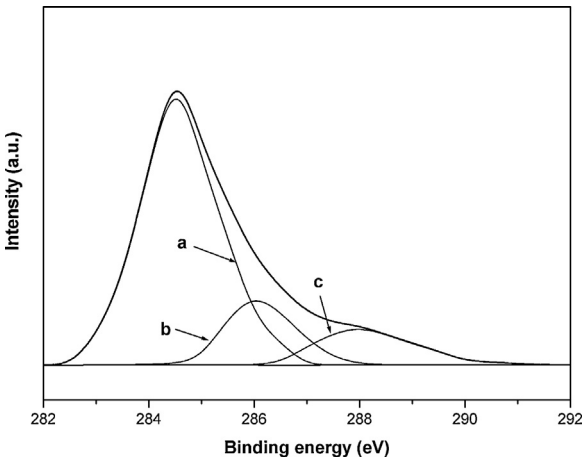

Fig. 4. C 1s XPS spectra of TiO_2–HPMC hybrid: (a) C–O, (b) C = O, (c) O–C = O.

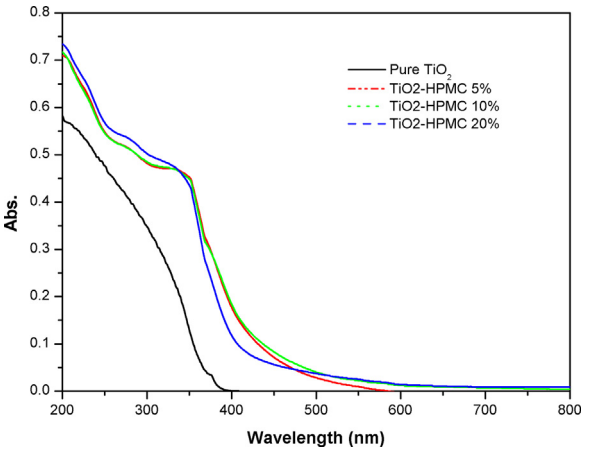

Fig. 5. (Color online). Diffuse reflectance spectra of prepared pure TiO_2 and TiO_2–HPMC hybrids.

Table 2
Band gap energies and absorption edges of prepared pure TiO_2 and TiO_2–HPMC hybrids calculated from the DRS spectra.

Samples	Band gap energy (eV)	Absorption edge (nm)
Pure TiO_2	3.115	398
TiO_2–HPMC 5%	2.397	517
TiO_2–HPMC 10%	2.405	515
TiO_2–HPMC 20%	2.507	494

hybridization. This could be assigned to TiO_2 containing localized oxygen vacancy located below the conduction band of TiO_2 [48,49], which therefore reduced the band gap. The band gap energy of the photocatalysts samples was determined from the equation, E_g (eV) = 1239.8/λ [50], where λ is the wavelength (nm) of the exciting light at the edge of absorption (Table 2). Also, it can be observed that the absorption intensity does not depend greatly on the HPMC-to-TiO_2 mass ratio. The best photocatalytic activity can be attained by the TiO_2–HPMC 5% sample. The above results indicate that HPMC is capable of sensitizing TiO_2 efficiently and the resulting composite photocatalysts can be excited by absorbing both UV and visible light to produce more electron–hole pairs and give a maximum visible light harvesting, which in turn could result in higher photocatalytic activities; therefore, it could be a promising photocatalytic material for efficient use of light, especially sunlight.

3.6. Thermal stability

To investigate the thermogravimetric behavior of the TiO_2–HPMC 5% hybrid nanocomposite, TGA curves were recorded as shown in Fig. 6. Those of HPMC and of prepared pure TiO_2 are also presented for comparison. The small mass loss observed at 50–120 °C is related to the release of moisture from the samples. The thermal decomposition temperature of the HPMC was found to be 345 °C (Fig. 6a). The mass loss observed above 120 °C for pure titania (Fig. 6b) may be ascribed to the removal of residual organics and water. For the TiO_2–HPMC 5% nanocomposite (Fig. 6c), the combustion temperature drop between room temperature and 100 °C was attributable to the water vapor. The final mass percent of the TiO_2–HPMC 5% sample was 84.05%. This result indicates that the TGA mass loss corresponding to HPMC was 3.9%. It is slightly lower than the initial amount of HPMC incorporated during the preparation process.

3.7. Photocatalytic activity

The photocatalytic activity of the TiO_2–HPMC hybrids was estimated using the reaction of photodegradation of the 4-NP solution (10 ppm) under visible light. The 4-NP is a very difficult degradable and highly toxic organic pollutant. The TiO_2–HPMC composite could photodegrade the 4-NP under visible light irradiation. The results show that the in situ hybridization of TiO_2 with HPMC dramatically increase its photocatalytic activity. In order to monitor the gradual disappearance of 4-NP, a series of UV–vis spectra are recorded with increasing the illumination time. Typical spectra of 4-NP solutions irradiated in the presence of TiO_2–HPMC 5% are shown in Fig. 7. Since spectra are recorded at pH = 9, the characteristic absorption of 4-NP appears at 401 nm, indicating the formation of phenolate ions. Fig. 7 shows that this characteristic disappears gradually and becomes weak after 180 min of visible light illumination. In addition, no other peak corresponding to possible intermediates is detected, perhaps due to the latter's low concentrations.

Compared with pure TiO_2, the TiO_2–HPMC catalysts exhibit a significant increase in 4-NP photodegradation efficiency, as shown in Fig. 8. Thereby, maximal photodegradation efficiencies of 85, 70, and 75% are achieved after 180 min of visible light irradiation in the presence of TiO_2–HPMC 5%, TiO_2–HPMC 10%, and TiO_2–HPMC 20%, respectively, whereas, only 37% of the initial concentration of 4-NP are photodegraded in the presence of pure TiO_2. Thus, the degradation efficiency of TiO_2 is improved almost 2 times after in situ hybridization with HPMC. Besides, the mineralization degree of 4-NP is checked by measuring the

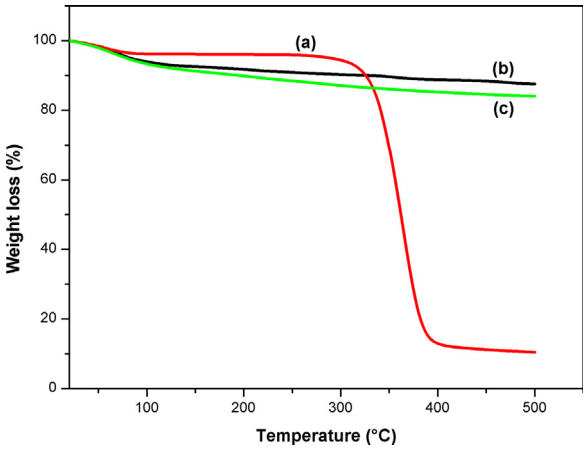

Fig. 6. (Color online). TGA curves: (a) HPMC, (b) prepared TiO_2, and (c) TiO_2–HPMC 5%.

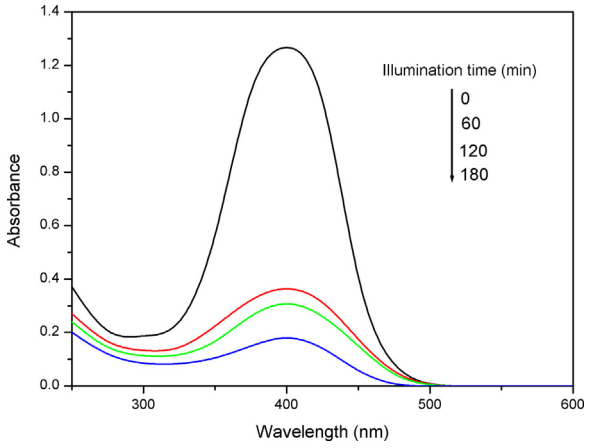

Fig. 7. (Color online). UV–vis absorption spectra of 4-NP at different intervals (C_0 = 10 ppm, catalyst: TiO_2–HPMC 5%).

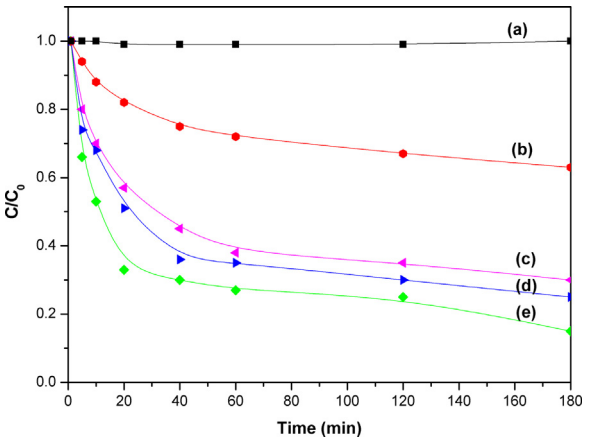

Fig. 8. (Color online). Photodegradation curves of 4-NP under visible irradiation 180 min, (a) photolysis (blank test), (b) pure TiO_2, (c) TiO_2–HPMC10%, (d) TiO_2–HPMC 20% and (e) TiO_2–HPMC 5%.

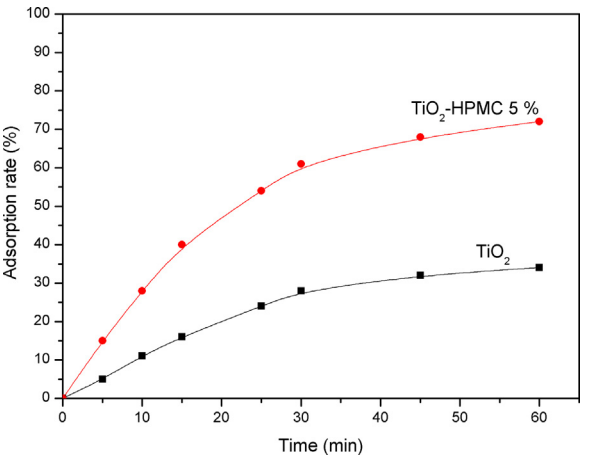

Fig. 9. (Color online). Adsorption curves of 4-NP on pure TiO_2 and TiO_2–HPMC 5%.

reduction in the TOC during the photodegradation process. It was found that the TOC removal of 4-NP after 180 min reached 72, 59, 61, and 22% in the presence of TiO_2–HPMC 5%, TiO_2–HPMC 10%, TiO_2–HPMC 20% and pure TiO_2, respectively. Three factors can be considered to explain the difference in activity between pure TiO_2 and TiO_2–HPMC hybrids:

- the enhancement of surface coverage of 4-NP on the photocatalyst;
- an acceleration of the migration rate of 4-NP to the surface of the photocatalyst;
- an expansion of the wavelength response range.

The surface coverage of organic pollutants on the catalysts is the key factor that dominates the photocatalytic efficiency of heterogeneous photocatalysis [51]. The surface coverage of 4-NP on the photocatalysts at fixed pH is mainly related to their specific surface areas. TiO_2–HPMC hybrids have high specific surface areas, which are around 200 $m^2 g^{-1}$ against only 53 $m^2 g^{-1}$ for pure TiO_2. These materials are mesoporous, and consequently they are expected to adsorb larger amounts of 4-NP than pure TiO_2. This is confirmed by measuring the adsorbed amount of 4-NP on the hybrid TiO_2–HPMC 5% on and pure TiO_2 surfaces after 60 min under dark. As shown in Fig. 9, the adsorption efficiency of 4-NP by TiO_2 is enhanced from 34% to 72% through hybridization with HPMC 5%, which means that the surface coverage of 4-NP on TiO_2 is enhanced more than two times, mainly by the OH group interaction that increases with the surface area. Then, TiO_2–HPMC hybrids are used as adsorbents and photocatalysts in this photochemical reaction system. Moreover, in situ prepared hybrids are composed of crystallites with an average size of about 5 nm, smaller than that of pure TiO_2. A small crystallite size gives rise to a large number of particles, which act as OH generators. The OH radicals are mainly formed after reaction of the photogenerated holes (h^+) with the H_2O and –OH groups adsorbed at the TiO_2 surface [52]. Besides, the in situ synthesis method is expected to provide organic–inorganic interpenetrating networks; thus, the –OH groups of the HPMC partner could also contribute to the formation of OH radicals. Accordingly, the number of OH radicals produced by the photoactivated TiO_2–HPMC hybrids is more important and for that reason, their photocatalytic activity is higher compared with that of pure TiO_2. Likewise, 4-NP molecules adsorb on the active sites (h^+) to form $C_6H_4NO_3$ radicals. Thus, the OH radicals, which are strong oxidizers, react with the adsorbed $C_6H_4NO_3$ radicals to form lower molecular weight degradation products [52].

On the other hand, the migration rate of 4-NP to the surface of the photocatalyst is strongly dependent on the 4-NP/photocatalyst interaction. This interaction is mainly governed by the pH of the solution. Many properties related to the photodegradation process such as the photocatalyst's surface charge state and the dissociation of the pollutant are dominated by the pH of the solution. In neutral media, TiO– is the predominant group on TiO_2–HPMC hybrid particles and 4-NP is present in the molecular form ($pK_a = 8.3$). This is because the interaction and affinity between photocatalyst particles and 4-NP are mainly governed by hydrogen bonding simply. Since the number of hydroxyl groups enabling the formation of hydrogen bonds in the photocatalyst/4-NP interface is higher in the TiO_2–HPMC hybrid particles compared with pure TiO_2, thus, an increase of the adsorbed amount and an enhancement of the photodegradation rate are expected to occur with hybrid materials.

Furthermore, the UV–vis diffuse reflection spectra (DRS) showed that TiO_2–HPMC hybrids prepared in situ absorb visible light in the range from 400 to 600 nm, unlike pure TiO_2. Accordingly, because most of the light is not in the UV range, the photodegradation efficiency of pure TiO_2 is relatively low. This is another parameter favoring the photodegradation efficiency of TiO_2–HPMC hybrids.

On the other hand, the number of hydroxyl groups does not explain alone the difference in the photodegradation

efficiency between the hybrid photocatalysts when the HPMC weight ratio varies. Thus, the specific surface area, the pore volume, the pore size and the visible light absorption should be considered to explain the higher photocatalytic efficiency observed with TiO_2–HPMC 5%.

3.7.1. Effect of the initial concentration of 4-NP

The photodegradation efficiency of 4-NP at different initial concentrations (5, 10, 15 and 20 ppm) by TiO_2–HPMC 5% hybrid material after 180 min of visible irradiation is shown in Fig. 10. Although the fraction of the unreacted 4-NP (i.e., C/C_0) increases with increasing C_0 using 1 g L^{-1} of TiO_2–HPMC 5%, the absolute amount of 4-NP degraded (i.e., C_0–C) actually increases (Table 3). The photodegradation reaction may be controlled by the number of surface sites on TiO_2–HPMC 5% particles.

Evidently, the amounts of 4-NP degraded under visible light by TiO_2–HPMC 5% increase with increasing initial concentrations; nevertheless their photodegradation rates decrease with initial concentrations. The present results, which are consistent with previous trends [53,54], indicate that the photocatalytic degradation process is rather promising at lower reactant concentrations.

In order to further investigate the kinetics of the photocatalytic degradation of 4-NP in the presence of TiO_2–HPMC 5% composite irradiated by visible light, the rate constant (k) of the degradation reaction has been studied in relation to the initial concentration of 4-NP solution (C_0). Table 3 reports the values of k resulting from the plot of $\ln(C_0/C)$ versus time for the photocatalytic degradation of 4-NP, which decreases as the initial reactant concentration increases. This can be ascribed to the decrease in the number of active sites on the catalyst's surface due to the covering of the surface with 4-NP molecules, which is directly proportional to the initial concentration of 4-NP. The experimental data have been rationalized in terms of the modified form of the Langmuir–Hinshelwood (L–H) kinetic model to describe the solid–liquid reaction successfully. The effect of initial

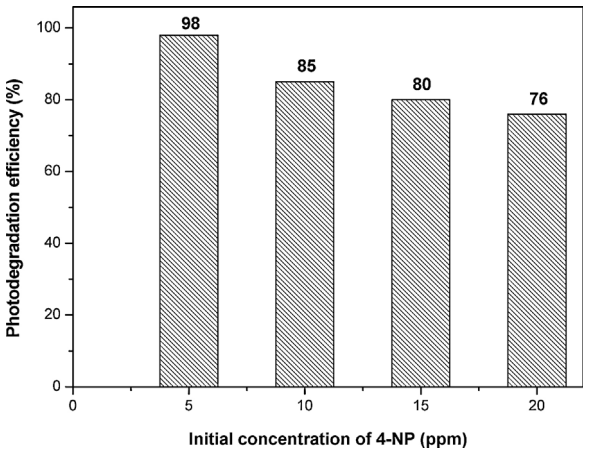

Fig. 10. Effect of the initial 4-NP concentration on its photodegradation efficiency after 180 min of visible irradiation in the presence of TiO_2–HPMC 5%.

Table 3
The absolute amount of 4-NP degraded according to the initial concentration C_0 and the corresponding rate constant k.

C_0 (ppm)	C_0–C (ppm)	k (min^{-1})
5	4.9	0.09
10	8.5	0.06
15	12	0.04
20	15.6	0.03

concentration of organic substrate on the initial degradation rate (r) is given by the following equations:

$$r = K_{LH}\, k_c\, [C]\, (1 + K_{LH}\, [C_0])^{-1} = k\, [C]$$

$$1/k = 1/K_{LH}\, k_c + [C_0]/k_c$$

where K_{LH} and k_c are the L–H adsorption equilibrium constant and rate constant of the surface reaction, respectively. At concentrations up to 20 mg L^{-1}, the applicability of the L–H equation for the photocatalytic degradation of 4-NP has been confirmed by the linear plot obtained by plotting the reciprocal of the rate constant ($1/k$) against the initial concentration ($[C]_0$) (not shown here). The values of K_{LH} and k_c are found to be 0.526 (mg^{-1} L) and 0.685 mg L^{-1} min^{-1}, respectively.

3.7.2. Effect of the preparation method

The preparation method of the TiO_2–HPMC hybrids can have a great effect on their photocatalytic activities. To evaluate this cause, the TiO_2–HPMC 5% hybrid was also prepared by the impregnation method, where a desired amount of prepared pure TiO_2 was dispersed for 30 min in an aqueous solution of HPMC and then filtered and dried. The subsequent analyses show that the TiO_2–HPMC 5% synthesized by the impregnation method has a specific surface area of 97 m^2 g^{-1} and a band gap of 2.9 eV. These characteristics are different from those obtained for the same nanocomposite prepared by the in situ pathway. As a result, TiO_2–HPMC 5% synthesized by the impregnation method has a capacity of pollutant adsorption and ability of visible light absorption weaker than that of TiO_2–HPMC 5% prepared by the in situ method. In addition, if a hybrid nanocomposite is prepared by a mechanical mixing of TiO_2 powders and cellulose solution, it is expected to obtain oxide nanoparticles poorly retained by cellulose [55]. On the other hand, the hybrid synthesized by the in situ pathway would benefit from the synergistic effect of the physical and chemical interactions between the organic and inorganic components and therefore could be used as an efficient photocatalyst [30]. Thus, the difference between both samples in the photodegradation efficiency of 4-NP after 180 min of visible light irradiation (Fig. 11) could be explained accordingly.

3.7.3. Photostability of the TiO_2–HPMC

To evaluate the photocatalytic stability of the hybrid photocatalyst, TiO_2–HPMC 5% was used in several photocatalytic runs, and each run lasted 180 min. After the first run, the photocatalyst was separated and used immediately for further runs without any treatment. The results

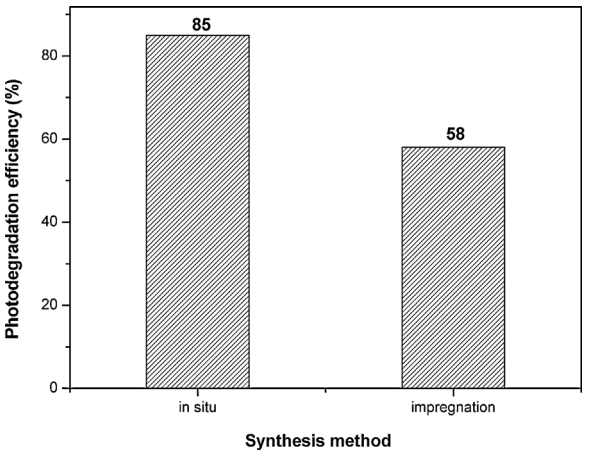

Fig. 11. Effect of the preparation method of TiO_2–HPMC 5% on the photodegradation efficiency of 4-NP after 180 min of visible irradiation (C_0 = 10 ppm).

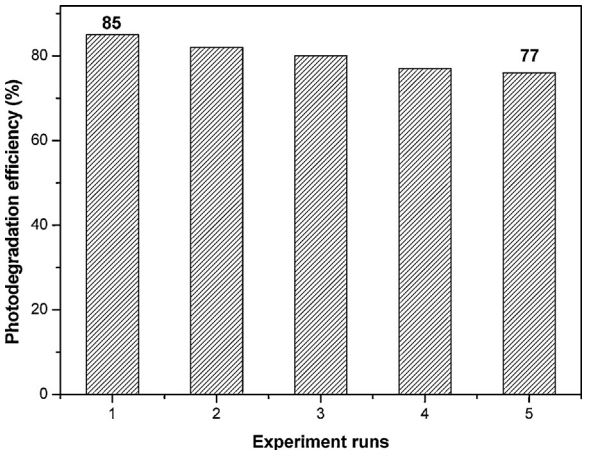

Fig. 12. Effect of number of runs on 4-NP degradation over TiO_2–HPMC 5% hybrid photocatalyst after 180 min (C_0 = 10 ppm).

displayed in Fig. 12 show that the hybrid photocatalyst is reusable and that it can also maintain high activity after several experimental runs. Only a gradual loss of photocatalytic activity can be observed after each run, and 77% of 4-NP degradation is still achieved after five runs. The decrease of photocatalytic activity after each run is possibly due to slight aggregation of nanoparticles and the gradual photocatalytic degradation of HPMC during the photocatalytic process. Hence, it is suggested that the in situ synthesis of TiO_2–HPMC hybrid materials endowed the TiO_2 nanoparticles with good stability against photocorrosion [56] compared with pure TiO_2.

4. Conclusion

TiO_2–HPMC hybrid photocatalysts were prepared by a simple in situ solution method. As the organic partner, HPMC can increase the surface area and extend the photoresponse of TiO_2 to the visible region. This leads to the improvement of the photocatalytic efficiency of TiO_2 nanoparticles under visible light. The degradation of 4-NP in an aqueous solution under visible light was carried out to evaluate the photocatalytic activity of the resulting composite photocatalysts. TiO_2–HPMC composite photocatalysts with certain HPMC-to-TiO_2 weight ratios (5, 10 and 20%) show higher photocatalytic activity than pure TiO_2 under visible light; TiO_2–HPMC 5% achieved the best performance. This can be attributed to the enhancement of surface coverage of 4-NP on the photocatalyst, accelerating the migration rate of 4-NP toward the surface of the photocatalyst, and expanding the wavelength response range. Also, the composite photocatalysts have good photocatalytic stability and can be reused five times with only gradual loss of activity.

References

[1] P. Gómez-Romero, C. Sanchez, Functional Hybrid Materials, Wiley-VCH, Weinheim, Germany, 2004.
[2] B.L. Su, C. Sanchez, X.Y. Yang, Hierarchically Structured Porous Materials: From Nanoscience to Catalysis, Separation, Optics and Life Science, Wiley-VCH, Weinheim, Germany, 2011.
[3] C. Boissière, D. Grosso, A. Chaumonnot, L. Nicole, Adv. Mater. 23 (2011) 599.
[4] I. Fechete, Y. Wang, J.C. Védrine, Catal. Today 189 (2012) 2–27.
[5] I. Fechete, P. Caullet, E. Dumitriu, V. Hulea, H. Kessler, Appl. Catal. A: Gen. 280 (2005) 245–254.
[6] I. Fechete, B. Donnio, O. Ersen, T. Dintzer, A. Djeddi, F. Garin, Appl. Surf. Sci. 257 (2011) 2791–2800.
[7] R.A. Sheldon, C. R. Acad. Sci. Paris, Ser. IIc 3 (2000) 541–551.
[8] I. Fechete, E. Gautron, E. Dumitriu, D. Lutic, P. Caullet, H. Kessler, Rev. Roum. Chim. 53 (2008) 49–54.
[9] C. Sanchez, G.J. de, A.A. Soler-Illia, F. Ribot, T. Lalot, C.R. Mayer, V. Cabuil, Chem. Mater. 13 (2001) 3061–3083.
[10] P. Gómez-Romero, Adv. Mater. 13 (3) (2001) 163–174.
[11] K.H. Haas, Adv. Eng. Mater. 2 (2000) 571–582.
[12] M.S. Yen, M.C. Kuo, Dyes Pigments 94 (2012) 349–354.
[13] J. Zhou, S. Liu, J. Qi, L. Zhang, J. Appl. Polym. Sci. 101 (2006) 3600–3608.
[14] Y. Tao, J. Pan, S. Yan, B. Tang, L. Zhu, Mater. Sci. Eng. B 138 (2007) 84–89.
[15] L. Nicole, L. Rozes, Adv. Mater. 22 (2010) 3208.
[16] C. Sanchez, L. Rozes, F. Ribot, C. Laberty-robert, D. Grosso, C. Sassoye, C. Boissiere, L. Nicole, C. R. Chimie 13 (2010) 3.
[17] A. Corma, U. Díaz, T. García, G. Sastre, A. Velty, J. Am. Chem. Soc. 132 (2010) 15011–15021.
[18] L. Pasqua, F. Testa, R. Aiello, S. Cundari, J.B. Nagy, Micropor. Mesopor. Mater. 103 (2007) 166–173.
[19] T. Takahashi, Y. Yamada, K. Kataoka, Y. Nagasaki, J. Control. Release 107 (2005) 408–416.
[20] L.T.T. Kim, O. Sel, C. Debiemme-Chouvy, C. Gabrielli, C. Laberty-Robert, H. Perrot, C. Sanchez, Electrochem. Commun. 12 (2010) 1136.
[21] N. Thanh-Dinh, Coll. Surf. B: Biointer. 103 (2013) 326–344.
[22] K. Nakata, A. Fujishima, J. Photochem. Photobiol. C: Photochem. Rev. 13 (2012) 169–189.
[23] N. Venkatachalam, M. Palanichamy, V. Murugesan, Mater. Chem. Phys. 104 (2007) 454–459.
[24] D. Morselli, F. Bondioli, M. Sangermano, M. Messori, Polymer 53 (2012) 283–290.
[25] J. Kim, S. Yun, Z. Ounaies, Macromol. 39 (12) (2006) 4202–4206.
[26] S. Yun, J. Kim, K.S. Lee, Int. J. Prec. Eng. Manuf. 11 (6) (2010) 987–990.
[27] E. Lam, K.B. Male, J.H. Chong, A.C.W. Leung, J.H.T. Luong, Trends Biotechnol. 30 (5) (2012) 283–290.
[28] R.J.B. Pinto, P.A.A.P. Marques, A.M. Barros-Timmons, T. Trindade, C.P. Neto, Compos. Sci. Technol. 68 (2008) 1088–1093.
[29] G. Goncalves, P.A.A.P. Marques, C.P. Neto, T. Trindade, M. Peres, T. Monteiro, Cryst. Growth Design 9 (2009) 386–390.
[30] J. Virkutyte, V. Jegatheesan, R.S. Varma, Bioresour. Technol. 113 (2012) 288–293.
[31] F. Wesarg, F. Schlott, J. Grabow, H.-D. Kurland, N. Heßler, D. Kralisch, F.A. Muller, Langmuir 28 (2012) 13518–13525.
[32] J. Zeng, S. Liu, J. Cai, L. Zhang, J. Phys. Chem. C 114 (2010) 7806–7811.
[33] T. Kunitake, S.W. Lee, Anal. Chim. Acta 504 (2004) 1–6.
[34] S.X. Li, F. Zheng, S. Cai, W. Liang, Y. Li, Sensor Actuator B: Chem. 188 (2013) 280–285.

[35] S.X. Li, F.Y. Zheng, X.L. Liu, F. Wu, N.S. Deng, J.H. Yang, Chemosphere 61 (4) (2005) 589–594.
[36] S.X. Li, S.J. Cai, F.Y. Zheng, Dyes Pigments 95 (2012) 188–193.
[37] A. Djeddi, I. Fechete, F. Garin, Top. Catal. 55 (2012) 700–709.
[38] M. Almáši, V. Zeleňák, R. Gyepes, A. Zukal, J. Čejka, Coll. Surf. A: Physicochem. Eng. Aspects 437 (2013) 101–107.
[39] S.K. Parayil, H.S. Kibombo, R.T. Koodali, Catal. Today 199 (2013) 8–14.
[40] A. Boulaoued, I. Fechete, B. Donnio, M. Bernard, P. Turek, F. Garin, Micropor. Mesopor. Mater. 155 (2012) 131–142.
[41] E. Dumitriu, V. Hulea, I. Fechete, C. Catrinescu, A. Auroux, J.-F. Lacaze, C. Guimon, Appl. Catal. A: Gen. 181 (1999) 15–28.
[42] P. Gorska, A. Zaleska, E. Kowalska, T. Klimczuk, J.W. Sobczak, E. Skwarek, W. Janusz, J. Hupka, Appl. Catal. B: Environ. 84 (2008) 440–447.
[43] S. Mun, Y. Chen, J. Kim, Sensor Actuator B: Chem. 171–172 (2012) 1186–1191.
[44] Z. Wu, F. Dong, W. Zhao, H. Wang, Y. Liu, B. Guan, Nanotechnology 20 (2009) 235701.
[45] I. Fechete, O. Ersen, F. Garin, L. Lazar, A. Rach, Catal. Sci. Technol. 3 (2013) 444–453.
[46] S. Haddoum, I. Fechete, B. Donnio, F. Garin, D. Lutic, C.E. Chitour, Catal. Commun. 27 (2013) 141–147.
[47] L. Zhang, H.H. Mohamed, R. Dillert, D. Bahnemann, J. Photochem. Photobiol. C: Photochem. Rev. 13 (2012) 263–276.
[48] I. Nakamura, N. Negishi, S. Kutsuna, T. Ihara, S. Sugihara, K. Takeuchi, J. Mol. Catal. A: Chem. 161 (2000) 205–212.
[49] Q. Xiao, J. Zhang, Sol. Energy 82 (8) (2008) 706–713.
[50] G. Cao, Y. Li, Q. Zhang, H. Wang, J. Hazard. Mater. 178 (1–3) (2010) 440–449.
[51] S.X. Li, F.Y. Zheng, C. Wen-Lian, H. Ai-Qin, X. Yu-Kun, J. Hazard Mater. 135 (1–3) (2006) 431–436.
[52] L. Tasseroul, S.L. Pirard, S.D. Lambert, C.A. Páez, D. Poelman, J.P. Pirard, B. Heinrichs, Chem. Eng. J. 191 (2012) 441–450.
[53] C. Hu, Y.Z. Wang, H.X. Tang, Chemosphere 41 (2000) 1205–1209.
[54] A. Di paola, V. Augugliaro, L. Palmisano, E. Savinov, J. Photochem. Photobiol. A: Chem. 155 (2003) 207–214.
[55] G. Goncalves, P.A.A.P. Marques, R.J.B. Pinto, T. Trindade, C.P. Neto, Compos. Sci. Technol. 69 (7–8) (2009) 1051–1056.
[56] J. Huang, T. Kunitake, J. Am. Chem. Soc. 125 (2003) 11834.